Biogeosciences

Deploying four optical UAV-based sensors over grassland: challenges and limitations

S. K. von Bueren[1,*]**, A. Burkart**[2,*]**, A. Hueni**[3]**, U. Rascher**[2]**, M. P. Tuohy**[1]**, and I. J. Yule**[1]

[1]Institute of Agriculture & Environment, Massey University, Palmerston North, New Zealand
[2]Institute of Bio- and Geosciences, IBG-2: Plant Sciences, Forschungszentrum Jülich GmbH, Jülich, Germany
[3]Remote Sensing Laboratories, University of Zurich, Zurich, Switzerland
[*]These authors contributed equally to this work.

Correspondence to: A. Burkart (an.burkart@fz-juelich.de)

Abstract. Unmanned aerial vehicles (UAVs) equipped with lightweight spectral sensors facilitate non-destructive, near-real-time vegetation analysis. In order to guarantee robust scientific analysis, data acquisition protocols and processing methodologies need to be developed and new sensors must be compared with state-of-the-art instruments. Four different types of optical UAV-based sensors (RGB camera, converted near-infrared camera, six-band multispectral camera and high spectral resolution spectrometer) were deployed and compared in order to evaluate their applicability for vegetation monitoring with a focus on precision agricultural applications. Data were collected in New Zealand over ryegrass pastures of various conditions and compared to ground spectral measurements. The UAV STS spectrometer and the multispectral camera MCA6 (Multiple Camera Array) were found to deliver spectral data that can match the spectral measurements of an ASD at ground level when compared over all waypoints (UAV STS: $R^2 = 0.98$; MCA6: $R^2 = 0.92$). Variability was highest in the near-infrared bands for both sensors while the band multispectral camera also overestimated the green peak reflectance. Reflectance factors derived from the RGB ($R^2 = 0.63$) and converted near-infrared ($R^2 = 0.65$) cameras resulted in lower accordance with reference measurements. The UAV spectrometer system is capable of providing narrow-band information for crop and pasture management. The six-band multispectral camera has the potential to be deployed to target specific broad wavebands if shortcomings in radiometric limitations can be addressed. Large-scale imaging of pasture variability can be achieved by either using a true colour or a modified near-infrared camera.

Data quality from UAV-based sensors can only be assured, if field protocols are followed and environmental conditions allow for stable platform behaviour and illumination.

1 Introduction

In the last decade, the use of unmanned aerial vehicles (UAVs) as remote sensing platforms has become increasingly popular for a wide range of scientific disciplines and applications. With the development of robust, autonomous and lightweight sensors, UAVs are rapidly evolving into stand-alone remote sensing systems that deliver information of high spatial and temporal resolution in a non-invasive manner. UAV systems are particularly promising for precision agriculture where spatial information needs to be available at high temporal frequency and spatial resolution in order to identify in-field variability (Stafford, 2000; Seelan et al., 2003; Lelong et al., 2008; Nebiker et al., 2008; Link et al., 2013). Zhang and Kovacs (2012) provide a comprehensive review of unmanned aerial systems applied in precision agriculture.

Precision agriculture aims at identifying crop and soil properties in near-real-time (Lebourgeois et al., 2012; Primicerio et al., 2012a) and at delivering results to farmers and decision makers with minimum delay to enable management decisions based on current crop and soil status. The use of input resources such as fertilizers, herbicides or water (Van Alphen and Stoorvogel, 2000; Carrara et al., 2004; Chávez et al., 2010) are matched to the current demand by the crops,

leading to an economical use of resources. The use of UAV-based sensors to detect water stress and quantify biomass and nitrogen content in crops and grasses has been demonstrated (Berni et al., 2008, 2009; Kawamura et al., 2011). Yield forecasting in wheat (Jensen et al., 2007) and rice (Swain et al., 2010), rangeland management (Rango et al., 2009), leaf area index (LAI) and green normalized difference vegetation index (NDVI) estimation in winter wheat (Hunt et al., 2010) and site-specific vineyard management (Turner, 2011; Primicerio et al., 2012b) have been accomplished using unmanned aerial platforms.

Proximal remote sensing methods can be used to detect pasture and crop biophysical parameters such as biomass, dry matter, fibre content, organic matter digestibility and macronutrient availability (nitrogen, phosphorus and potassium). Pasture monitoring approaches capable of measuring biophysical variables over the whole farm at a high spatial resolution allow for site-specific management decisions and optimum nutrient management (Sanches et al., 2012). While vegetation indices have been frequently applied for biomass and dry matter estimation (Mutanga, 2004; Duan et al., 2011; Vescovo et al., 2012), waveband-specific algorithms have been developed to estimate macronutrients (Mutanga and Skidmore, 2007; Pullanagari et al., 2012a, b).

In a pasture management context in New Zealand, where air- and spaceborne remote sensing methods are often limited by frequent cloud cover, UAV-based remote sensing can potentially overcome some of those limitations. Recent developments in commercially available lightweight and small digital cameras and multispectral sensors support precision nutrient management. However, these sensors need to be characterized and validated against state-of-the-art reference instruments. The extraction of quantitative information relies on thorough calibration procedures, good instrument characterization and a high standard of field operation.

Various studies have specifically evaluated multispectral sensors and consumer-grade digital cameras and assessed their potential for vegetation monitoring. The use of a conventional, ground-based broadband digital RGB camera has shown limited success in estimating green biomass on shortgrass prairie, suggesting that narrow-band sensors are more promising for application over such complex ecosystems (Vanamburg et al., 2006). An image processing workflow for three consumer digital cameras has been developed by Lebourgeois et al. (2012) and they have suggested that the cameras have a high potential for terrestrial remote sensing of vegetation due to their versatility and multispectral capabilities. Vegetation indices derived from visible and near-infrared imagery acquired by two compact digital cameras were found to generate strong relationships with crop biophysical parameters and to be practical for monitoring of temporal changes in crop growth (Sakamoto et al., 2012). Kelcey and Lucieer (2012) developed a processing chain to improve the imagery acquired with the same six-band multispectral sensor that was used in the current study. They showed that image quality can be improved through application of sensor correction techniques to facilitate subsequent image analysis. A novel, UAV-based lightweight high-resolution spectrometer, which was tested in the field for the first time in the current study, was introduced by Burkart et al. (2013). Nijland et al. (2014) evaluated the use of near-infrared (NIR) and RGB cameras for the use of vegetation monitoring and plant phenology trend detection and found that the NIR-converted cameras were outperformed by standard RGB cameras. Poor band separation and the limited dynamic range of the NIR camera system limited the use of the sensors for vegetation monitoring in a controlled laboratory and in a field experiment.

Studies usually deploy a single UAV sensing system over an area of interest. But because different agricultural applications and environmental frameworks demand specific capabilities of an UAV remote sensing system, the current study uses four different sensors over the same experimental area to evaluate each sensor's suitability for applied grassland monitoring. From preliminary experiments, it was evident that the UAV system, including platform and sensor, need to be specifically matched to the vegetation parameter to be investigated. The present study used two compact digital cameras (RGB and NIR), a six-band multispectral camera (visible/near-infrared – VNIR) and a high-resolution spectrometer (VNIR) mounted on two different UAV platforms to acquire spectral information over dairy pastures in order to characterise each instrument in terms of radiometric quality and accuracy of spectral information obtainable, as compared to a ground reference instrument. Handling and limitations of the UAVs, flight planning, field procedures and the capabilities of the different sensors are discussed as a prospective guideline for upcoming UAV sensor-based research. Results are evaluated with a focus on inter-sensor comparability, aspects of field data collection using UAVs and the sensor's capabilities for monitoring green vegetation.

1.1 Experimental site

The experimental flight campaign was conducted in February 2013 on a Massey University dairy farm near Palmerston North, New Zealand, (No. 1 Dairy, located at lat. -40.376, long. 175.606). No. 1 Dairy is a fully operational dairy farm with an effective area of 119.7 ha. UAV flights were performed over four different paddocks with distinct characteristics from bare soil to dry and irrigated ryegrass pasture. At the time of data acquisition between 11:00 and 15:00 LT no clouds were visible.

1.2 UAV systems

As shown in Table 1, two different UAV systems were used: a QuadKopter (MikroKopter), owned and operated by Massey University, and a Falcon-8 (AscTec (Ascending Technologies), Krailing, Germany), from the Research Centre Jülich,

Table 1. UAV platforms.

Name	QuadKopter	Falcon-8
Manufacturer	MikroKopter	Ascending Technologies
Weight [g]	1900	1800
Max. Payload [g]	1000	500
Power source	LiPo, 4200 mAh, 14.8 V	Lipo, 6400 mAh, 11.1 V
Endurance [min]	12	15
GPS navigation	Ublox LEA 6s GPS chip	Ublox LEA 6T
Features	Open Source Gyro-stabilized camera mount	Stabilized camera mount, live video link, motor redundancy
Sensors	MCA6	UAV STS, RGB, Canon IR

Germany. The Falcon-8 uses the AscTec Autopilot Control V1.68 software. It has two identical exchangeable gimbals manufactured by AscTec, one for the Sony camera the other one for the spectrometer and Canon camera. Both gimbals are dampened and actively stabilized in pitch and roll. The MikroKopter UAV was fitted with an AV130 Standard Gimbal produced by Photo Higher. The gimballed camera mounts levelled out any platform movement to ensure the sensors were pointing in nadir direction to the ground at all times during the flight. The main difference between the Falcon-8 and the MikroKopter platforms is the payload restriction, which precludes the Falcon-8 from lifting sensors heavier than 0.5 kg, thus making it necessary to use the MikroKopter UAV to lift the Mini-MCA6 sensor. Both UAVs with their payloads were intensively tested on multiple flights before the study.

1.3 UAV sensors

Four UAV sensors (Fig. 1) were tested and compared in terms of their ability to produce reflectance data over pastures. All of the sensors were lighter than 1 kg including batteries and were either modified or specifically designed for use on remotely controlled platforms. The sensors share a spectral range in the VNIR which is considered the most relevant region of the electromagnetic spectrum for agricultural research applications (Lebourgeois et al., 2008). In terms of spatial and spectral resolution (Fig. 2), the sensors differ significantly. Table 2 lists their relevant properties.

Mini-MCA6 (MCA6): the Mini-MCA6 (Multispectral Camera Array) is a six-band multispectral camera (Tetracam, Chatsworth, CA, USA) that can acquire imagery in six discrete wavebands. A camera-specific image alignment file is provided by the manufacturer. Exchangeable filters in the range of 400 to 1100 nm can be fitted to six identical monochromatic cameras. Table 3 lists the filter setup used during the study. The camera firmware allows pre-setting all imaging related parameters such as exposure time, shutter release interval and image format and size. Six two gigabyte CompactFlash memory cards store up to 800 images (10 bit RAW format, full resolution). With an opening angle of 38.3° × 31.0°, the camera has a relatively narrow field of

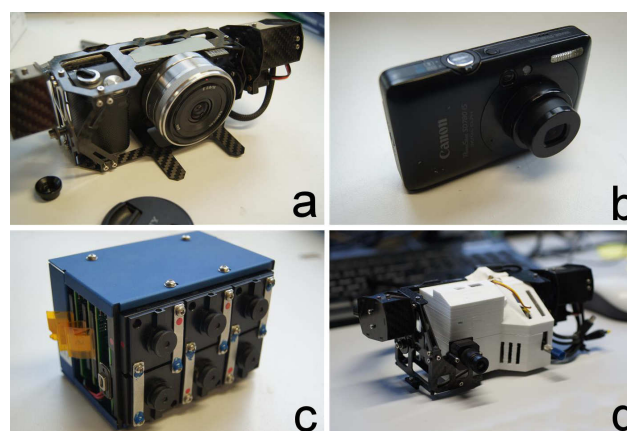**Figure 1.** UAV-based sensors: **(a)** Sony Nex5n RGB camera **(b)** Canon PowerShot IR camera **(c)** MCA6 multispectral camera **(d)** Spectrometer (UAV STS).

view as opposed to the Canon and Sony cameras. The camera was set to a 2 ms exposure time and was run on a 2 s shutter release interval with images saved in the 10 bit RAW format. Positioning of the camera was achieved by hovering the UAV over the vegetation target for at least 30 s per waypoint.

STS spectrometer (UAV STS): the spectrometer was adapted for UAV-based remote sensing at the Research Centre Jülich. Its design is based on the STS VIS spectrometer (Ocean Optics, Dunedin, FL, USA) with the addition of a micro-controller to enable remote triggering and saving of spectral data. The spectrometer operated on an independent power source and its low weight and fine spectral resolution made it ideal for use on an UAV. The full specifications, calibration efforts and validation of the STS spectrometer are presented in Burkart et al. (2013). An identical spectrometer, on the ground, acquired spectra of incoming radiance every time the airborne sensor was triggered. Spectra were saved on a micro SD card.

Sony RGB camera: a SONY Nex5n (Sony Corporation, Minato, Japan) modified by AscTec was attached to the Falcon-8 using a specially designed camera mount. A live video feed from the camera to the UAV operator and remote triggering were available. Spectral sensitivity was given by
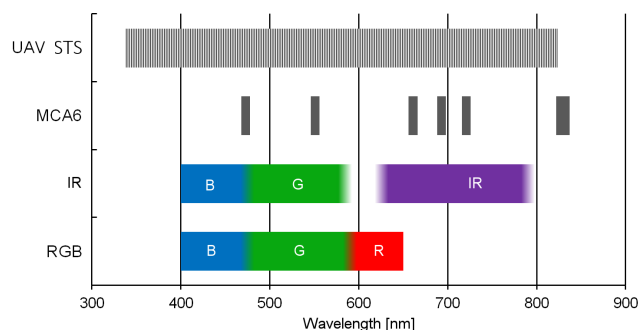
Figure 2. Spectral sensitivity of the four sensors. Spectral bands are indicated by different colours.

the common Bayer matrix (Bayer, 1976; Hirakawa et al., 2007) and hot mirror used in consumer digital cameras.

Canon PowerShot camera: the Canon PowerShot SD780 IS is a consumer digital camera that has been professionally (LDP LLC, Carlstadt, US) converted to acquire near-infrared imagery. The near-infrared filter has been replaced with a red-light-blocking filter. Again, the spectral response of the camera is based on the Bayer pattern colour filter array. Customized CHDK (Canon Hack Development Kit) firmware allows running the camera in a continuous capture mode at specific time intervals (2 s, user defined). Camera acquisition was set to automatic as time constraints and UAV batteries did not allow for accurate manual configuration of white balance, aperture, ISO and shutter speed. Images were saved as JPEGs. A live video link from the UAV's on-board camera enabled precise positioning of the RGB and infrared cameras over the ryegrass pastures. The main difference to the MCA6 is the inability to adjust filter settings and the camera's bandwidths. According to manufacturer information each band has an approximate width of 100 nm.

1.4 Ground-based sensors

ASD HandHeld 2 ground-based reference sensor: ground-based spectral measurements were acquired with an ASD HandHeld 2 portable spectroradiometer (Analytical Spectral Devices, Inc., Boulder, Colorado, US). The device covers a spectral range from 325 nm to 1075 nm which makes it suitable for comparison with all UAV sensors flown in this study. At 700 nm the device has a spectral resolution of 3 nm and the field of view equates to 25°. A Spectralon® panel (Spectralon®, Labsphere, Inc., North Sutton, NH, USA) was used to acquire white reference measurements before each target measurement. Each target was measured 10 times from 1 m distance while moving over the area of interest.

1.5 Flight planning and data acquisition procedure

Taking into account the operational requirements of each sensor and flying platform, a detailed flight plan was developed. Eight sampling locations defined by waypoints were

selected from overview images and supported by an in situ visual assessment of the paddock. A focus was put on covering a wide range of pasture qualities from dry to fully irrigated ryegrass pastures. Waypoints were selected in paddock areas with homogeneous pasture cover. This ensured that each waypoint can be considered representative for the area of the paddock it is located in, and it aided dealing with the different sensor footprint sizes (Table 4).

Each sampling location was marked with a tarpaulin square, which was clearly visible in all spectral bands of the aerial images. In order to avoid interference effects of the markers with the UAV STS measurements, they were removed before acquisition of spectra. Next to the first waypoint, a calibration site with coloured tarpaulin squares was set-up and measured with the ASD HandHeld 2.

The sensors were flown over the targets in the following order: (1) RGB camera for an overview shot, (2) IR camera for an overview shot, (3) MCA6 over calibration sites (black, grey, white and red tarpaulins black foam material, bare soil) and waypoints and (4) UAV spectrometer over waypoints. Overview images cover all sampling locations in an area with a single shot from 100 to 150 m flying height. MCA6 images were taken from 25 m above the ground. UAV STS data were collected from a height of 10–15 m, and 15 spectra were taken over each waypoint. During the experiment, the Falcon-8 was flown in semi-autonomous GPS mode. Coordinates of the sampling locations were recorded with a low-accuracy GPS (Legend, HTC, Taoyuan, Taiwan). The Falcon-8 used those coordinates to autonomously reach the marker locations. Over each sampling location, the flight mode was then switched to manual and the UAV was positioned over the target as accurately as possible using a live video link. The UAV STS and the live camera were on the same stabilized gimbal and aligned in a way, that the centre of the FPV camera approximates the UAV STS's field of view. The QuadKopter was flown in manual mode during the entire experiment. In test flights preceding this experiment, it was found that the GPS on board of the MikroKopter was not accurate enough to position the sensor over a waypoint.

Flights were conducted consecutively to minimize variability due to changing illumination and vegetation status. Figure 3 depicts raw data from the imaging sensors before any processing has been applied. Before the flight of the UAV spectrometer, ASD ground reference measurements were taken at each waypoint.

1.6 Data processing

Data from each sensor underwent calibration and correction procedures.

MCA6: a proprietary software package (PixelWrench2 by Tetracam) that was delivered with the Tetracam was used to transfer images from the CompactFlash memory cards to the computer. Each RAW band was processed to a TIFF (Tagged Image File Format) image in order to identify all images that

Table 2. Sensor properties.

Name	Sony Nex5n RGB	Canon Powershot IR	MCA6	STS
Company	Sony – modified	Canon – modified	Tetracam	Ocean Optics – modified
Type	RGB camera integrated	VIS + Infrared camera in the Falcon-8 UAV	Multispectral Imager with 6 bands of 10 nm width	Spectroradiometer with additional electronics for remote control
Field of View	$73.7° \times 53.1°$	$57.2° \times 40°$	$38.3° \times 31.0°$	$12°$
Spectral bands	3	3	6	256
Spectral range	Blue, Green, Red	Blue, Green, IR	450–1000 nm	338–824 nm
Image size	4912×3264	4000×3000	1280×1024	n/a
Image format	JPEG	JPEG	RAW	n/a
Dynamic Range	8 bit	8 bit	10 bit	14 bit
Weight [g]	500	100	790	216
Handling	Wireless trigger, live view	Interval mode	Interval mode	Wireless trigger, live view

Table 3. MCA6 filter specifications.

	Slave 1	Master	Slave 2	Slave 3	Slave 4	Slave 5
Centre wavelength FWHM (nm)	473	551	661	693	722	831
Bandwidth FWHM (nm)	9.26	9.72	9.73	9.27	9.73	17.81
Peak transmission (%)	64.37	72.54	61.4	66.89	63.63	65.72

show the target area. As a result, between 6 and 15 images per target were found to be suitable for further image processing (total of 109 images) and two images showing the tarpaulin areas and bare soil were selected for reflectance factor calibration. From there, RAW image processing was done in Matlab (The MathWorks Inc., 2011). Both the calibration images and the vegetation target images were noise corrected and vignetting effects were removed for each of the six cameras (Yu, 2004; Olsen et al., 2010; Kelcey and Lucieer, 2012). A sensor correction factor was applied to each filter based on filter sensitivity factory information (Kelcey and Lucieer, 2012).

UAV STS: as described in Burkart et al. (2013) a temperature-based dark current correction (Kuusk, 2011) and an inter-calibration of the air- and ground-based spectrometer were applied before derivation of reflectance factors.

Sony RGB Camera: the red, green and blue bands were calibrated to a reflectance factor with the empirical line method (Smith and Milton, 1999; Baugh and Groeneveld, 2008) relating the ASD reflectance over the coloured reference tarpaulins (Fig. 3) to real reflectance (Aber et al., 2006).

Canon infrared camera: the camera was corrected using the same method as for the RGB camera, but with the centre wavelengths adapted to the infrared sensitive pixels.

The images that show the tarpaulin and the bare soil were selected as calibration images and processed separately. The white and the red tarpaulins were excluded from analysis due to pixel saturation and high specular reflection. For each of the calibration surfaces (black, grey, black foam and bare soil) a subset image area was defined from which the pixel values for the empirical line method were derived.

For each calibration target, ten ASD reference spectra were convolved to the spectral response of the Mini-MCA6 (see Spectral Convolution). The empirical line method was applied to establish band-specific calibration coefficients. Using those coefficients, the empirical line method was applied to each vegetation target image on a pixel-by-pixel basis, thus converting digital numbers of the image pixels to a surface reflectance factor.

In order to extract the footprint area over which ground ASD and UAV spectrometer data had been acquired, the relevant image area was identified and extracted from each image by identifying the markers in the image. Footprints were matched between sensors by defining a 0.3 by 0.3 m area below the waypoint marker as the region of interest. An average reflectance factor was calculated for each footprint resulting in between 6 and 15 values per sample location for the MCA6 images. Standard deviations, mean and median were calculated for each waypoint.

ASD HandHeld 2 ground reference sensor: ASD HandHeld 2 spectral binary files were downloaded and converted to reflectance using the HH2Sync software package (Version 1.30, ASD Inc.). Spectral data were then imported into the spectral database SPECCHIO (Hueni et al., 2009).

Spectral Convolutions: in order to synthesize STS spectrometer data from ground-based ASD data, a discrete spectral convolution was applied (Kenta and Masao, 2012). Each STS band was convolved by applying Eq. (1), using a Gaussian function to represent the spectral response function of each STS band. These spectral response functions (SRFs) were parameterized by the calibrated centre wavelengths of the STS instrument and by a nominal FWHM (full width at half maximum) of 3 nm for all spectral bands. The discrete

Table 4. Optical sensor footprint properties.

	UAV STS	MCA6	Canon IR	Sony RGB	ASD
Footprint shape	Circular	Rectangular	Rectangular	Rectangular	Circular
Footprint size [Sensor height (m)]	Ø 2.1 m [10]	17.3 × 13.9 m [25]	109.0 × 72.8 m [100]	149.9 × 99.9 m [100]	Ø 0.44 m [1]
Number of pixels	n/a	1280 × 1024	4000 × 3000	4912 × 3264	n/a
Ground resolution (m)	n/a	0.0135	0.0273	0.0305	n/a
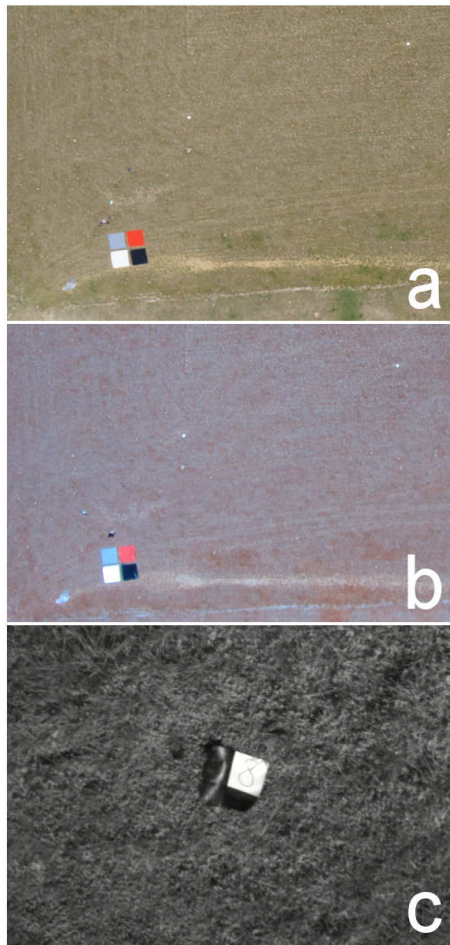
Figure 3. Raw data from the imaging sensors **(a)** RGB camera at 100 m altitude, **(b)** IR camera at 100 m altitude, **(c)** MCA6 at 25 m altitude (red band). The images show the region of interest cropped from a larger image. White points represent the tarpaulin waypoint markers.

convolution range (nm) of each band was based on ±3σ of the Gaussian function and applied at the wavelength positions where an ASD band occurred, i.e. at every nanometre. It must be noted that the results of this convolution cannot truly emulate the actual system response of the STS as the ASD sampled input spectra are already a discrete representation of the continuous electromagnetic spectrum and are hence already inherently smoothed by the measurement process of the ASD.

In a similar manner, MCA6 bands were simulated, but having replaced the Gaussian assumption of the SRFs with the spectral transmission values (Table 3) digitized from analogue figures supplied by the filter manufacturer (Andover Corporation, Salem, US).

$$R_k = \frac{\sum_{j=n}^{m} c_j R_j}{\sum_{j=n}^{m} c_j}, \tag{1}$$

where R_k = reflectance factor of Ocean Optics band k, R_j = reflectance factor of ASD band j, c_j = weighting coefficient based on the Ocean Optics STS, spectral responsivity at wavelength of ASD band j, $n : m$ = convolution range of Ocean Optics band k.

2 Results

MCA6 and UAV STS: calibrated reflectance factors of the UAV spectrometer and the MCA6 were compared to calculated ASD reflectance values using linear regression analysis. The UAV STS and the ASD HandHeld 2 were compared over the whole STS spectrum, while the MCA6 was compared to the ASD in its six discrete bands.

Figure 4 shows the spectral information derived from both the STS spectrometer and MCA6 in direct comparison with the convolved ASD-derived reflectance spectra for two distinctively different waypoints in terms of ground biomass cover and greenness of vegetation. Waypoint 2 is a recently grazed pasture with a high percentage of dead matter and senescent leaves. Soil background reflectance was high and the paddock was very dry, with no irrigation scheme operating. Pasture at waypoint 8 had not been grazed recently and therefore vegetation cover was dense with a mix of ryegrass pastures and clover. The paddock undergoes daily irrigation and no soil background signal was detectable. The data indicated that the MCA6 estimates higher reflectance factors than the UAV spectrometer and the ASD for the blue, green and the lowest red band. In the far-red and NIR bands, values were consistently lower than those derived from the ASD but still higher than reflectance measured by the UAV STS. While the ASD detected a steep increase in reflectance in the
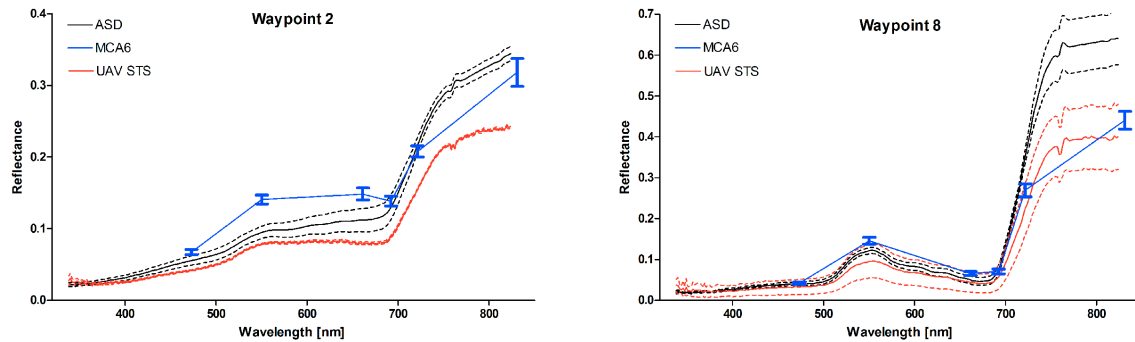
Figure 4. Reflectance of the spectral sensors ASD (black), MCA6 (blue) and UAV STS (red) as measured over the exemplary waypoints 2 and 8. SD in dotted lines for the ASD and UAV STS and with error bars for the 6 bands of the MCA6.

Table 5. Correlation matrix of the optical sensors (R^2). Values were calculated for corresponding bands of each sensor pair over all waypoints. Number of images (n) is given in brackets.

	RGB	IR	MCA6	UAV STS
RGB	1			
IR	0.913 (16)	1		
MCA6	0.377 (16)	0.945 (16)	1	
UAV STS	0.681 (24)	0.891 (24)	0.826 (48)	1
ASD	0.674 (24)	0.647 (24)	0.924 (48)	0.978 (3856)

Figure 5. Reflectance comparison of UAV-based sensors to convolved ASD-derived reflectance showing data over all eight sample locations and spectra (MCA6 $n = 48$, STS $n = 120$). MCA6 vs. ASD (blue): $R^2 = 0.92$, slope of linear regression: 0.6691, offset: 0.0533. STS vs. ASD (red): $R^2 = 0.98$, slope of linear regression: 0.6522, offset: 0.0142.

red edge, both UAV sensors detected a lower signal in the same region of the spectrum.

The mean MCA6-derived spectra showed an increase in reflectance in the green peak region of the vegetation spectrum that is approximately 0.05 % higher than in the same region of the UAV spectrometer. The slope between the green and the red bands is positive for both sensors demonstrating the dried, stressed state of the vegetation at waypoint 2. While MCA6 bands show low correlations with the UAV STS and the ASD for the 551 nm and the 661 nm bands, its values are in line with the other sensors in the red-edge region of the spectra.

The MCA6 correlates significantly with ASD-derived reflectance (R^2 0.92, Fig. 5, Table 5) when compared over all eight waypoints and over all six-bands ($n = 48$). Shortcomings of spectral accuracy of the MCA6 are revealed when comparing band reflectance values over different sample locations and per waypoint (Fig. 6). The green band (551 nm) achieves lowest correlations with ASD convolved reflectance values ($R^2 = 0.68$), with MCA6 reflectance factors overestimated for all waypoints. The remaining five bands show correlations with R^2 between 0.70 (722 nm) and 0.97 (661 nm). Overall, the MCA6 overestimates bands below the red edge, while it shows low deviations from the STS- and the ASD-derived reflectance values for the red-edge bands. Due to the low number of waypoints, the blue-, green- and red-band correlations need to be interpreted with caution. With an
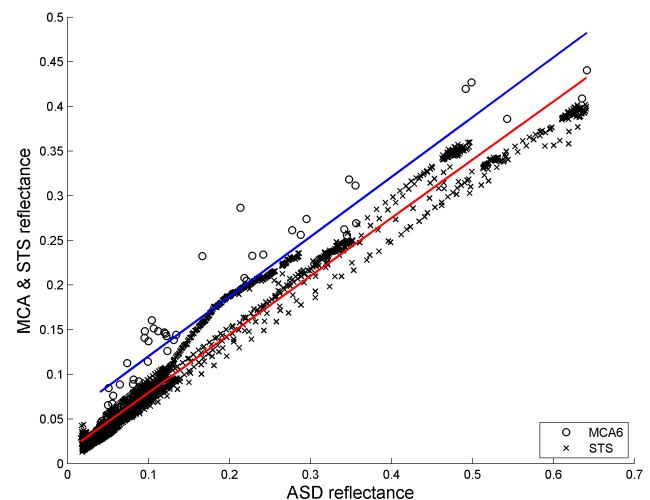
R^2 of 0.98, the UAV spectrometer strongly correlates to the reflectance derived from the ASD when compared over all waypoints (Table 4). Even though the trend of the spectra is similar to the ASD ground truth, differences are visible in the magnitude of the reflectance mainly in the near-infrared.

RGB and NIR camera: as can be seen in Table 4, the correlation between the RGB and IR cameras results in an R^2 of 0.91, whereas the correlations to the high-resolution spectrometers are as low as 0.65 between the NIR camera and the ASD. The RGB camera and MCA6 are poorly correlated with a R^2 of 0.38.
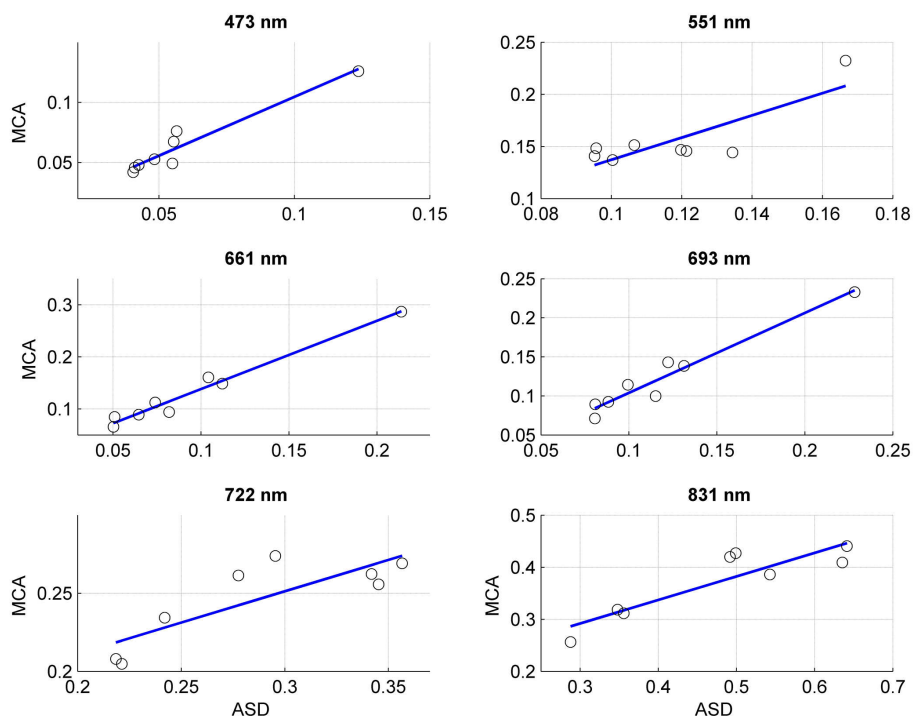
Figure 6. Comparison of reflectance values between MCA6 and convolved ASD reflectance for each MCA6 band. 473 nm: $R^2 = 0.93$, regression slope (RS): 0.9783; 551 nm: $R^2 = 0.68$, RS: 1.0654; 661 nm: $R^2 = 0.97$, RS: 1.311; 693 nm: $R^2 = 0.95$, RS: 1.0225; 722 nm: $R^2 = 0.7$, RS: 0.4009; 831 nm: $R^2 = 0.8$, RS: 0.4516.

3 Discussion

MCA6: when compared to the UAV spectrometer and the ground reference data, the MCA6 filters performed well in the red-edge region of the electromagnetic spectrum. This observation is supported by the CMOS sensor relative sensitivity which is over 90 % in the red-edge and the near-infrared bands according to factory information (Tetracam Inc.). The largest deviations were observed in the green band, where the MCA6 consistently overestimates vegetation reflectance factors. In sample locations with low biomass cover and/or stressed pastures, this results in a negative slope between the red bands. The sensor's performance is further impaired when high soil background reflectance is present, as is the case for the first three waypoints and the bare soil calibration target. While the green peak in the UAV STS and ASD measurements is barely visible over waypoint 2 but pronounced for waypoint 8, the MCA does not pick up on that feature. Green-band reflectance is overestimated for the drier pasture, while deviations from the other sensors' measurements over irrigated, greener pasture are lower. Those differences must be put down to radiometric inconsistencies in the MCA6 and potential calibration issues and it suggests that with the current filter setup, the MCA6 cannot be regarded as suitable for remote sensing of biochemical constituents and fine-scale monitoring of vegetation variability. Another complexity can be seen in the near-infrared regions of the derived spectra. For the UAV STS, MCA6 and the ASD, the variability of measured reflectance factors increases. This discrepancy is likely to arise from a combination of areas of different spatial support in terms of the sensor's field-of view (FOV) and calibration biases (sensor and reflectance calibration). Further investigation into sensor performance over targets with complex spectral behaviour must be conducted in order to evaluate the spectral performance of those bands. The number of waypoints visited was not high enough to fully assess the performance of the four lower MCA6 bands as can be seen in Fig. 6. Due to the statistical distribution of the data points, a definite statement on the performance of those bands is not possible. The empirical line method used for reflectance calibration introduces further errors because only one calibration image was acquired over the entire measurement procedure. Reflectance factor reliability can be improved by more frequent acquisition of calibration images.

UAV STS: the UAV STS-delivered spectra with strong correlations to the ASD measurements. The calculation of narrow-band indices or spectral fitting algorithms is thus possible. However, depending on the status of the vegetation target the ASD-derived reflectance factors can be up to 1.5 times (Fig. 4) higher than the UAV STS measurements. This result, particularly striking in the NIR, is below expectations, as Burkart et al. (2013) compared the Ocean Optics spectrometer (UAV STS) to an ASD Field Spec 4 and reported good agreements between the two instruments. The

main source of discrepancies between the ASD and STS measurements can be attributed to inconsistencies in footprint matching due to using a live feed from a camera that can only approximate the spectrometer's field of view. By choosing homogeneous surfaces and averaging over multiple measurements, parts of the problems arising from footprint were addressed in this study. However the matching of the footprint of two different spectrometers can go beyond comparing circles and rectangles due their optical path as recently shown by MacArthur et al. (2012). A more thorough inter-comparison of the ASD and the particular Ocean Optics device employed on the UAV will be required in the future.

RGB and NIR cameras: an empirical line calibration was used for the reflectance factor estimation of both consumer RGB and infrared-modified cameras. Although correlations between the digital cameras and the high-resolution spectrometers exist, they must be treated with caution. This is due to the unknown radiometric response of the cameras, band overlaps and the inherent differences between simple digital cameras and numerical sensors. Both cameras provide imagery with high on-ground resolution, thus enabling identification of in-field variations. In terms of the NIR camera, the wide bandwidth and limited information on the spectral response call for cautious use and further evaluation if the camera is to be used for quantitative vegetation monitoring. At this stage, this study can only suggest that the sensor might be used for support of visual paddock assessment and broadband vegetation indices. Nevertheless, the results demonstrate the opportunities these low-budget sensors offer for simple assessment of vegetation status over large areas using UAVs. If illumination conditions enable an empirical line calibration, reasonable three-band reflectance results can be calculated. Further improvements of radiometric image quality can be expected from fixed settings of shutter speed, ISO, white balance and aperture, as well as for the use of the RAW format. A calibration of lens distortion and vignetting parameters could further increase the quality, especially in the edges of the image (Yu, 2004). However, operational efficiency increases with automatic camera settings which only varied minimally due to the stable illumination conditions at the time of the study.

The empirical line method that was used for reflectance calibration was based on some simplifications. Variations in illumination and atmospheric conditions require frequent calibration image acquisition in order to produce accurate radiometric calibration results. Due to the conservative management of battery power and thus relatively short flight times, only one MCA6 flight was conducted to acquire an image of the calibration tarpaulins and the bare soil. The same restriction applies to the quality of the radiometric calibration of the RGB and IR camera. The use of colour tarpaulin surfaces as calibration targets has implications on the quality of the achieved reflectance calibration in this study. Although they provide low-cost and easy-to-handle calibration surfaces, they are not as spectrally flat as would be needed for

a sensor calibration with minimum errors. Moran et al. (2001, 2003) have investigated the use of chemically treated canvas tarpaulins and painted targets in terms of their suitability as stable reference targets for image calibration to reflectance and introduce measures to ensure optimum calibration results. They concluded that specially painted tarps could provide more suitable calibration targets for agricultural applications.

Discrepancies in measured reflectance factors between the UAV STS, the MCA6 and the ASD arise from a combination of factors. Foremost, inherent differences in their spectral and radiometric properties lead to variations in measured reflectance factors. Deviations in footprint matching between the STS spectrometer and the ground measurements, although kept to a minimum, lead to areas of different spatial support and cannot be fully eliminated. Another dimension to this complexity is added by the UAVs and the camera gimbals. Although platform movements were minimal due to the stable environmental conditions and the compensation of any small platform instabilities by the camera gimbals, a small variability in measured radiant flux must be attributed to uncertainties in sensor viewing directions. For a complete cross-calibration between the UAV-based and ground sensors, these potential error sources need to be quantified. Within the context of evaluating sensors for their usability and potential for in-field monitoring of vegetation, those challenges were not addressed in the current study.

In-field data acquisition and flight procedures, one of the key challenges in accommodating four airborne sensors over the same area of interest is accurate footprint matching and minimizing any errors that are introduced by this complexity. Camera gimbals, on board GPS software, piloting skills and waypoint selection maximized footprint matching between sensors. The Falcon-8 UAV was capable of a very stable hover flight over the area of interest while the MikroKopter UAV required manual piloting to ensure that it hovered over the area of interest. The tarpaulin markers were invaluable as a visual aid both during piloting of the UAVs and during subsequent image processing for identifying the footprint areas in each image. Because of the need to select waypoints that were representative for a large area of the paddock, the stable hovering behaviour of the Falcon-8 ensured that the UAV spectrometer's footprint was comparable to the other sensors' field of view. Although the described measures and precautions enabled confident matching of footprints, they can only be applied when working in homogeneous areas of pasture and vegetation cover. Confounding factors, such as soil background influence, large variations in vegetation cover inside the footprint area and strong winds that destabilise the platform, will compromise accurate footprint matching.

When acquiring data with UAVs, responses to changes in environmental conditions, such as increasing wind speeds and cloud presence, need to be immediate. Although specifications from UAV manufacturers attest that the flying vehicles are able to cope with winds of up to $30\,\mathrm{km\,h^{-1}}$, in reality

the wind speed at which a flight must be interrupted is considerably lower. Platform stability, altitude control and footprint matching accuracy between sensors are compromised under high winds. The fact that two different UAV platforms had been used potentially introduces more variability that cannot be quantified. However, the aforementioned payload restrictions make the use of two different platforms inevitable. Due to the fast progress in UAV platform development, this intricacy is likely to be irrelevant in the future as platforms become more versatile and adaptable to accommodate various sensor requirements.

Technical specifications of UAVs: both UAVs were powered with lithium polymer (LiPo) batteries. A fully charged battery enabled flying times of approximately 10 min for the payload carried. With only four batteries available for each UAV, this lead to a data acquisition time frame of about 40 min per flying platform. However, because turbulence, unplanned take offs and landings and inaccurate GPS positions frequently required revisiting a waypoint, the total number of sample locations that could be investigated between 11:00 and 15:00 LT when illumination conditions were most favourable, was low. This makes thorough flight planning, marking of waypoints and efficient collection of ground reference data essential. Due to the non-availability of power outlets and the time it takes to fully recharge a LiPo battery, battery life limits the time frame in which airborne data can be collected. At the time of the study, higher powered LiPo batteries were still too heavy, thus neutralizing a gain in flight time due to the high weight of the more powerful battery. Those restrictions can slow down data acquisition considerably and the number of ground sampling locations is limited. In the future, improvements in platform stability and electronics as well as higher powered batteries will enable larger ground coverage by UAVs. Using in-field portable charging options such as powered from car batteries can significantly enhance the endurance of rotary wing UAVs.

The evaluated UAV sensors differ in their suitability for deployment in vegetation monitoring and more specifically pasture management applications. While high spectral accuracy is essential for quantifying parameters such as nutritional status in crops and pastures, the high spatial resolution imaging ability of digital cameras can be used to assess paddocks and fields with regard to spatial variations that may not be visible to a ground observer.

Usability of sensors: the UAV STS spectrometer with its high spectral resolution can be used to derive narrowband vegetation indices such as the PRI (photochemical reflectance index) (Suarez et al., 2009) or TSAVI (transformed soil adjusted vegetation index) (Baret et al., 1989). Furthermore, its narrow bands facilitate identification of wavebands that are relevant for agricultural crop characterization (Thenkabail et al., 2002). Once those centre wavelengths have been identified, a more broadband sensor such as the MCA6 could target crop and pasture characteristics with specific filter setups provided the MCA6 performance can be enhanced in terms of radiometric reliability. The consumer digital cameras seem to be useful for derivation of broadband vegetation indices such as the green NDVI (Gitelson et al., 1996) or the GRVI (Motohka et al., 2010). Identification of wet and dry areas in paddocks and growth variations are further applications that such cameras can cover. Imaging sensors that identify areas in a paddock that need special attention are extremely useful, and although they do not provide the high spectral resolution of the UAV STS spectrometer, they do give a visual indication of vegetation status.

Challenges and limitations: deploying UAVs is a promising new approach to collect vegetation data. As opposed to ground-based proximal sensing methods, UAVs offer nondestructive and efficient data collection and less accessible areas can be imaged relatively easy. Moreover, UAVs can potentially provide remote sensing data when aircraft sensors and satellite imagery are unavailable. However, three main factors can cause radiometric inconsistencies in the measurements: sensors, flying platforms and the environment.

The sensors mounted on the UAVs introduce the largest level of uncertainty in the data. Radiometric aberrations across the camera lenses can be addressed by a flat fieldcorrection of the images.

Further factors are camera settings. In this study, shutter speed, exposure time and ISO were set on automatic because of the clear sky and stable illumination conditions. However, to facilitate extraction of radiance values and quantitative information on the vegetation, these settings need to be fixed for all the flights in order to make the images comparable.

The RAW image format is recommended when attempting to work with absolute levels of radiance as it applies the least alterations to pixel digital numbers.

Furthermore, footprint matching between sensors with different sizes and shapes is challenging. While it is straightforward for imaging cameras with rectangular shaped footprints, matching measurements between the UAV STS, ASD and the imaging sensors can only be approximated. While footprint shape is fixed, the size can be influenced by the flying altitude above ground.

However, it is also important to be aware of any bidirectional effects that are introduced as a result of the camera lens' view angle and illumination direction (Nicodemus, 1965).

Although UAV platforms are equipped with gyrostabilization mechanisms, GPS chips and camera gimbals, an uncertainty remains of whether the camera is in fact pointing nadir and at the target. Slight winds or a motor imbalance can destabilise the UAV system enough to cause the sensor field of view to be misaligned. For imaging sensors this is less of an issue as it is for numerical sensors such as the UAV STS. The live view will only ever be an approximation of the sensor's actual FOV. Careful setting up of the two systems on the camera gimbal and periodical measurement of known targets to align the spectrometer's FOV to the live view camera can help to minimise deviations between FOVs.

The environment also needs to be considered for the collection of robust radiometric data. Even if all other factors are perfect, winds or wobbling of the platform caused by, e.g., a motor imbalance or a bad GPS position hold can cause the sensor to direct its FOV to the wrong spot. In terms of the imaging cameras this is again simple to check after image download whereas the UAV STS data might possibly not show any deviations in the data.

With a good knowledge of the sensors characteristics and the necessary ground references an UAV operator will be able to acquire satisfying data sets, if the environmental conditions are opportune. Based on a tested UAV with known uncertainties in GPS and gimbal accuracy the data set can be quality flagged and approved for further analysis.

4   Conclusions

UAVs are rapidly evolving into easy-to-use sensor platforms that can be deployed to acquire fine-scale vegetation data over large areas with minimal effort. In this study, four optical sensors, including the first available UAV-based microspectrometer were flown over ryegrass pastures and cross-compared. Overall, the quality of the reflectance measurements of the UAV sensors is dependent on thorough data acquisition processes and accurate calibration procedures. The novel high-resolution STS spectrometer operates reliably in the field and delivers spectra that show high correlations to ground reference measurements. For vegetation analysis, the UAV STS holds potential for feature identification in crops and pastures as well as the derivation of narrow-band vegetation indices. Further investigations and cross-calibrations are needed, mainly with regard to the near-infrared measurements in order to establish a full characterization of the system. It was also demonstrated that the six-band MCA6 camera can be used as a low spectral resolution multispectral sensor with the potential to deliver high-resolution multispectral imagery. In terms of its poor radiometric performance in the green and near-infrared filter regions, it is evident that the sensor needs further testing and correction efforts to eliminate the error sources of these inconsistencies. Over sample locations with low vegetation cover and strong soil background interference, the MCA6 image data needs to be processed with caution. Individual filters must be assessed further, with a focus on the green and NIR regions of the electromagnetic spectrum. Any negative effects that depreciate data quality, such as potentially unsuitable calibration targets (coloured tarpaulins) need to be identified and further examined in order to guarantee high quality data. If those issues can be addressed and the sensor is equipped with relevant filters, the MCA6 can become a useful tool for crop and pasture monitoring. The modified Canon infrared and the RGB Sony camera have proven to be easy-to-use sensors that deliver instant high-resolution imagery covering a large spatial area. No spectral calibration has been performed on those sensors,

but factory spectral information allowed converting digital numbers to a ground reflectance factor. Near-real-time assessment of variations in vegetation cover and identification of areas of wetness/dryness as well as calculation of broadband vegetation indices can be achieved using these cameras. A number of issues have been identified during the field experiments and data processing. Exact footprint matching between the sensors was not achieved due to differences in the FOVs of the sensors, instabilities in UAV platforms during hovering and potential inaccuracies in viewing directions of the sensors due to gimbal movements. Although those differences in spatial scale reduce the quality of sensor intercomparison, it must be stated that under field conditions a complete match of footprints between sensors is not achievable. For the empirical line calibration method that was applied to the MCA6 and the digital cameras, we propose the use of spectrally flat painted panels for radiometric calibration rather than tarpaulin surfaces. To reduce complexity of the experiment and keep the focus on the practicality of deploying multiple sensors on UAVs, the influence of directional effects has been neglected.

The field protocols developed allow for straightforward field procedures and timely coordination of multiple UAV-based sensors as well as ground reference instruments. The more autonomously the UAV can fly, the more focus can be put on data acquisition. Piloting UAVs in a field where obstacles such as power lines and trees are present requires the full concentration of the pilot and at least one support person to observe the flying area. Due to technical restrictions, the total area that can be covered by rotary wing UAVs is still relatively small, resulting in a point sampling strategy. Higher powered, lightweight batteries on UAVs can allow for more frequent calibration image acquisition and the coverage of natural calibration targets, thus improving the radiometric calibration. Differences in UAV specifications and capabilities lead to the UAVs having a specific range of applications that they can undertake reliably.

As shown in this study even after calibration efforts, biases and uncertainties remain and must be carefully evaluated in terms of their effects on data accuracy and reliability. Restrictions and limitations imposed by flight equipment must be carefully balanced with scientific data acquisition protocols. The different UAV platforms and sensors each have their strengths and limitations that have to be managed by matching platform and sensor specifications and limitations to data acquisition requirements. UAV-based sensors can be quickly deployed in suitable environmental conditions and thus enable the timely collection of remote sensing data. The specific applications that can be covered by the presented UAV sensors range from broad visual identification of paddock areas that require increased attention to the identification of waveband-specific biochemical crop and pasture properties on a fine spatial scale. With the development of sensor-specific data processing chains, it is possible to generate data sets for agricultural decision making within a few

hours of data acquisition and thus enable the adjustment of management strategies based on highly current information.

Edited by: M. Rossini

This publication is supported by COST – www.cost.eu

References

Aber, J. S., Aber, S. W., Pavri, F., Volkova, E., and Penner II, R. L.: Small-format aerial photography for assessing change in wetland vegetation, Cheyenne Bottoms, Kansas, Transactions of the Kansas Academy of Science, 109, 47–57, doi:10.1660/0022-8443(2006)109[47:sapfac]2.0.co;2, 2006.

Baret, F., Guyot, G., and Major, D. J.: TSAVI: A Vegetation Index Which Minimizes Soil Brightness Effects On LAI And APAR Estimation, Geoscience and Remote Sensing Symposium, 1989, IGARSS'89, 12th Canadian Symposium on Remote Sensing, International, 1355–1358, 1989.

Baugh, W. M. and Groeneveld, D. P.: Empirical proof of the empirical line, Int. J. Remote Sens., 29, 665–672, doi:10.1080/01431160701352162, 2008.

Bayer, B. E.: Color imaging array, 1976.

Berni, J., Zarco-Tejada, P., Surez, L., González-Dugo, V., and Fereres, E.: Remote sensing of vegetation from uav platforms using lightweight multispectral and thermal imaging sensors, The International Archives of the Photogrammetry, Remote Sensing and Spatial Information Sciences, XXXVII, 2008.

Berni, J. A. J., Zarco-Tejada, P. J., Suarez, L., and Fereres, E.: Thermal and Narrowband Multispectral Remote Sensing for Vegetation Monitoring From an Unmanned Aerial Vehicle, Ieee T. Geosci. Remote, 47, 722–738, doi:10.1109/Tgrs.2008.2010457, 2009.

Burkart, A., Cogliati, S., Schickling, A., and Rascher, U.: A novel UAV-based ultra-light weight spectrometer for field spectroscopy, Sensors Journal, IEEE, 14, 62–67, doi:10.1109/jsen.2013.2279720, 2013.

Carrara, M., Comparetti, A., Febo, P., and Orlando, S.: Spatially variable rate herbicide application on durum wheat in Sicily, Biosys. Eng., 87, 387–392, 2004.

Chávez, J. L., Pierce, F. J., Elliott, T. V., Evans, R. G., Kim, Y., and Iversen, W. M.: A remote irrigation monitoring and control sys-

tem (RIMCS) for continuous move systems. Part B: Field testing and results, Precis. Agric., 11, 11–26, 2010.

Duan, M., Gao, Q., Wan, Y., Li, Y., Guo, Y., Ganzhu, Z., Liu, Y., and Qin, X.: Biomass estimation of alpine grasslands under different grazing intensities using spectral vegetation indices, Can. J. Remote Sens., 37, 413–421, 2011.

Gitelson, A. A., Kaufman, Y. J., and Merzlyak, M. N.: Use of a green channel in remote sensing of global vegetation from EOS-MODIS, Remote Sens. Environ., 58, 289–298, 1996.

Hirakawa, K., Wolfe, P. J., and Ieee: Spatio-spectral color filter array design for enhanced image fidelity, in: 2007 Ieee International Conference on Image Processing, Vols 1–7, IEEE International Conference on Image Processing ICIP, 645–648, 2007.

Hueni, A., Nieke, J., Schopfer, J., Kneubühler, M., and Itten, K. I.: The spectral database SPECCHIO for improved long-term usability and data sharing, Comput. Geosci., 35, 557–565, doi:10.1016/j.cageo.2008.03.015, 2009.

Hunt, E. R., Hively, W. D., Fujikawa, S. J., Linden, D. S., Daughtry, C. S. T., and McCarty, G. W.: Acquisition of NIR-Green-Blue Digital Photographs from Unmanned Aircraft for Crop Monitoring, Remote Sens., 2, 290–305, doi:10.3390/Rs2010290, 2010.

Jensen, T., Apan, A., Young, F., and Zeller, L.: Detecting the attributes of a wheat crop using digital imagery acquired from a low-altitude platform, Comput. Electron. Agr., 59, 66–77, doi:10.1016/j.compag.2007.05.004, 2007.

Kawamura, K., Sakuno, Y., Tanaka, Y., Lee, H.-J., Lim, J., Kurokawa, Y., and Watanabe, N.: Mapping herbage biomass and nitrogen status in an Italian ryegrass (Lolium multiflorum L.) field using a digital video camera with balloon system, J. Appl. Remote Sens., 5, 053562, doi:10.1117/1.3659893, 2011.

Kelcey, J. and Lucieer, A.: Sensor Correction of a 6-Band Multispectral Imaging Sensor for UAV Remote Sensing, Remote Sens., 4, 1462–1493, 2012.

Kenta, T. and Masao, M.: Radiometric calibration method of the general purpose digital camera and its application for the vegetation monitoring, Land Surf. Remote Sens., 8524, doi:10.1117/12.977211, 2012.

Kuusk, J.: Dark Signal Temperature Dependence Correction Method for Miniature Spectrometer Modules, J. Sens., 2011, 608157, 2011.

Lebourgeois, V., Bégué, A., Labbé, S., Mallavan, B., Prévot, L., and Roux, B.: Can commercial digital cameras be used as multispectral sensors? A crop monitoring test, Sensors, 8, 7300–7322, 2008.

Lebourgeois, V., Begue, A., Labbe, S., Houles, M., and Martine, J. F.: A light-weight multi-spectral aerial imaging system for nitrogen crop monitoring, Precis. Agric., 13, 525–541, doi:10.1007/s11119-012-9262-9, 2012.

Lelong, C. C. D., Burger, P., Jubelin, G., Roux, B., Labbe, S., and Baret, F.: Assessment of unmanned aerial vehicles imagery for quantitative monitoring of wheat crop in small plots, Sensors, 8, 3557–3585, doi:10.3390/S8053557, 2008.

Link, J., Senner, D., and Claupein, W.: Developing and evaluating an aerial sensor platform (ASP) to collect multispectral data for deriving management decisions in precision farming, Comput. Electron. Agr., 94, 20–28, doi:10.1016/j.compag.2013.03.003, 2013.

MacArthur, A., MacLellan, C. J., and Malthus, T.: The fields of view and directional response functions of two field spectroradiometers, IEEE Geosci. Remote Sens., 50, 3892–3907, 2012.

Moran, M. S., Bryant, R. B., Clarke, T. R., and Qi, J. G.: Deployment and calibration of reference reflectance tarps for use with airborne imaging sensors, Photogram. Eng. Rem. S., 67, 273–286, 2001.

Moran, S., Fitzgerald, G., Rango, A., Walthall, C., Barnes, E., Bausch, W., Clarke, T., Daughtry, C., Everitt, J., Escobar, D., Hatfield, J., Havstad, K., Jackson, T., Kitchen, N., Kustas, W., McGuire, M., Pinter, P., Sudduth, K., Schepers, J., Schmugge, T., Starks, P., and Upchurch, D.: Sensor development and radiometric correction for agricultural applications, Photogram. Eng. Rem. S., 69, 705–718, 2003.

Motohka, T., Nasahara, K. N., Oguma, H., and Tsuchida, S.: Applicability of green-red vegetation index for remote sensing of vegetation phenology, Remote Sensing, 2, 2369–2387, 2010.

Mutanga, O.: Hyperspectral remote sensing of tropical grass quality and quantity, Hyperspectral remote sensing of tropical grass quality and quantity, x + 195 pp.-x + 195 pp., 2004.

Mutanga, O. and Skidmore, A. K.: Red edge shift and biochemical content in grass canopies, ISPRS J. Photogram., 62, 34–42, doi:10.1016/j.isprsjprs.2007.02.001, 2007.

Nebiker, S., Annen, A., Scherrer, M., and Oesch, D.: A Lightweight Multispectral Sensor for Micro UAV – Opportunities for Very High Resolution Airborne Remote Sensing, XXI ISPRS Congress. Beijing, China, 2008.

Nijland, W., de Jong, R., de Jong, S. M., Wulder, M. A., Bater, C. W., and Coops, N. C.: Monitoring plant condition and phenology using infrared sensitive consumer grade digital cameras, Agr. Forest Meteorol., 184, 98–106, doi:10.1016/j.agrformet.2013.09.007, 2014.

Olsen, D., Dou, C., Zhang, X., Hu, L., Kim, H., and Hildum, E.: Radiometric Calibration for AgCam, Remote Sens., 2, 464–477, doi:10.3390/rs2020464, 2010.

Primicerio, J., Di Gennaro, S. F., Fiorillo, E., Genesio, L., Lugato, E., Matese, A., and Vaccari, F. P.: A flexible unmanned aerial vehicle for precision agriculture, Precis. Agric., 13, 517–523, doi:10.1007/s11119-012-9257-6, 2012a.

Primicerio, J., Di Gennaro, S. F., Fiorillo, E., Genesio, L., Lugato, E., Matese, A., and Vaccari, F. P.: A flexible unmanned aerial vehicle for precision agriculture, Precis. Agric., 13, 1–7, 2012b.

Pullanagari, R. R., Yule, I. J., Hedley, M. J., Tuohy, M. P., Dynes, R. A., and King, W. M.: Multi-spectral radiometry to estimate pasture quality components, Precis. Agric., 13, 442–456, doi:10.1007/s11119-012-9260-y, 2012a.

Pullanagari, R. R., Yule, I. J., Tuohy, M. P., Hedley, M. J., Dynes, R. A., and King, W. M.: In-field hyperspectral proximal sensing for estimating quality parameters of mixed pasture, Precis. Agric., 13, 351–369, doi:10.1007/s11119-011-9251-4, 2012b.

Rango, A., Laliberte, A., Herrick, J. E., Winters, C., Havstad, K., Steele, C., and Browning, D.: Unmanned aerial vehicle-based remote sensing for rangeland assessment, monitoring, and management, J. Appl. Remote Sens., 3, 033542, doi:10.1117/1.3216822, 2009.

Sakamoto, T., Gitelson, A. A., Nguy-Robertson, A. L., Arkebauer, T. J., Wardlow, B. D., Suyker, A. E., Verma, S. B., and Shibayama, M.: An alternative method using digital cameras for continuous monitoring of crop status, Agr. Forest Meteorol., 154, 113–126, doi:10.1016/j.agrformet.2011.10.014, 2012.

Sanches, I. D., Tuohy, M. P., Hedley, M. J., and Mackay, A. D.: Seasonal prediction of in situ pasture macronutrients in New Zealand pastoral systems using hyperspectral data, Int. J. Remote Sens., 34, 276–302, doi:10.1080/01431161.2012.713528, 2012.

Seelan, S. K., Laguette, S., Casady, G. M., and Seielstad, G. A.: Remote sensing applications for precision agriculture: A learning community approach, Remote Sens. Environ., 88, 157–169, 2003.

Smith, G. M. and Milton, E. J.: The use of the empirical line method to calibrate remotely sensed data to reflectance, Int. J. Remote Sens., 20, 2653–2662, doi:10.1080/014311699211994, 1999.

Stafford, J. V.: Implementing precision agriculture in the 21st century, J. Agr. Eng. Res., 76, 267–275, 2000.

Suarez, L., Zarco-Tejada, P. J., Berni, J. A. J., Gonzalez-Dugo, V., and Fereres, E.: Modelling PRI for water stress detection using radiative transfer models, Remote Sens. Environ., 113, 730–744, doi:10.1016/j.rse.2008.12.001, 2009.

Swain, K. C., Thomson, S. J., and Jayasuriya, H. P. W.: Adaption of an unmanned helicopter for low altitude remote sensing to estimate yield and total biomass of a rice crop, Trans. ASABE, 53, 21–27, 2010.

Thenkabail, P. S., Smith, R. B., and De Pauw, E.: Evaluation of narrowband and broadband vegetation indices for determining optimal hyperspectral wavebands for agricultural crop characterization, Photogram. Eng. Rem. S., 68, 607–621, 2002.

Turner, D. J.: Development of an Unmanned Aerial Vehicle (UAV) for hyper-resolution vineyard mapping based on visible, multispectral and thermal imagery, School of Geography & Environmental Studies Conference 2011, 2011.

Van Alphen, B. and Stoorvogel, J.: A methodology for precision nitrogen fertilization in high-input farming systems, Precis. Agric., 2, 319–332, 2000.

Vanamburg, L. K., Trlica, M. J., Hoffer, R. M., and Weltz, M. A.: Ground based digital imagery for grassland biomass estimation, Int. J. Remote Sens., 27, 939–950, doi:10.1080/01431160500114789, 2006.

Vescovo, L., Wohlfahrt, G., Balzarolo, M., Pilloni, S., Sottocornola, M., Rodeghiero, M., and Gianelle, D.: New spectral vegetation indices based on the near-infrared shoulder wavelengths for remote detection of grassland phytomass, Int. J. Remote Sens., 33, 2178–2195, doi:10.1080/01431161.2011.607195, 2012.

Yu, W.: Practical anti-vignetting methods for digital cameras, IEEE Transactions on Consumer Electronics, 50, 975–983, 2004.

Zhang, C. and Kovacs, J. M.: The application of small unmanned aerial systems for precision agriculture: a review, Precis. Agric., 13, 693–712, doi:10.1007/s11119-012-9274-5, 2012.